NANO · MICRO small
www.small-journal.com

Hollow Ptychography: Toward Simultaneous 4D Scanning Transmission Electron Microscopy and Electron Energy Loss Spectroscopy

Na Yeon Kim, Shaohong Cao, Karren L. More, Andrew R. Lupini, Jianwei Miao, and Miaofang Chi**

With the recent development of high-acquisition-speed pixelated detectors, 4D scanning transmission electron microscopy (4D-STEM) is becoming routinely available in high-resolution electron microscopy. 4D-STEM acts as a "universal" method that provides local information on materials that is challenging to extract from bulk techniques. It extends conventional STEM imaging to include super-resolution techniques and to provide quantitative phase-based information, such as differential phase contrast, ptychography, or Bloch wave phase retrieval. However, an important missing factor is the chemical and bonding information provided by electron energy loss spectroscopy (EELS). 4D-STEM and EELS cannot currently be acquired simultaneously due to the overlapping geometry of the detectors. Here, the feasibility of modifying the detector geometry to overcome this challenge for bulk specimens is demonstrated, and the use of a partial or defective detector for ptycholgaphic structural imaging is explored. Results show that structural information beyond the diffraction-limit and chemical information from the material can be extracted together, resulting in simultaneous multi-modal measurements, adding the additional dimensions of spectral information to 4D datasets.

1. Introduction

Recent detector developments have enabled 4 dimensional scanning transmission electron microscopy (4D-STEM), a data acquisition method that consists of collecting a set of diffraction patterns at each beam position in a scanned image, resulting in 4D datasets: 2D real space scanning coordinates and 2D diffraction space information.[1-5] 4D-STEM detectors can acquire nearly all exiting electrons after they interact with a specimen and offer advantages over monolithic hardware-based STEM detectors. All conventional STEM image contrast modes, such as bright field, annular bright field, and annular dark field etc., can be digitally generated by the application of virtual detectors. Therefore, 4D-STEM serves as a "universal" STEM method.[1,5] Second, compared to images that are integrated by conventional annular shaped detectors, the electron diffraction patterns acquired in 4D-STEM contain more information about the atomic potential, strain, magnetic field, and electrical field. By applying appropriate methods, such as ptychography, differential phase contrast (DPC), template matching, or Bloch wave reconstruction, structure and field information of specimens can be extracted. For example, electric and magnetic fields can be obtained based on 4D-STEM datasets.[3,5,6] Localized electron columns in electrides can be mapped at atomic resolution.[7] Recent reports also show that both light and heavy elements can be simultaneously observed using 4D-STEM, which is important for energy materials that contain light ions, such as Li^+ and H^+.[8,9] Advantages of using 4D-STEM for lattice strain analysis have been shown.[1,10] More importantly, a 4D dataset provides an opportunity to quantitively characterize the sample by deconvolving the electron probe using electron ptychography methods, opening numerous new opportunities for materials research such as imaging beam sensitive materials with significantly reduced electron dose,[11,12] super-high spatial resolution,[13] and improved noise rejection and sensitivity.[14]

Ptychography is a scanning coherent diffractive imaging technique that retrieves both the complex object transmission function and the illumination function from a sequence of 2D diffraction patterns.[15–17] There are several advantages of ptychography as compared to conventional techniques. The most obvious advantage is that the reconstructed spatial resolution from ptychography is not directly limited by the real space beam scanning step size or beam spot size, as DPC or HAADF (High Engle Annular Dark Field) imaging would be. In realistic situations, the spatial resolution of ptychography is limited by the collection angle and wavelength, while with super-resolution methods, the

N. Y. Kim, J. Miao
Department of Physics and Astronomy and California NanoSystems Institute
University of California
Los Angeles, CA 90095, USA
S. Cao, K. L. More, A. R. Lupini, M. Chi
Center for Nanophase Materials Sciences
Oak Ridge National Laboratory
Oak Ridge, TN37831, USA
E-mail: arl1000@ornl.gov; chim@ornl.gov

The ORCID identification number(s) for the author(s) of this article can be found under https://doi.org/10.1002/smll.202208162

DOI: 10.1002/smll.202208162

reconstructed resolution can be extended further beyond the diffraction limit according to the redundancy in the dataset. In principle, ptychography is able to achieve wavelength-limited resolution provided that, 1) the detector is big enough to collect all the relevant scattering and able to ensure a reasonable sampling in reciprocal space; 2) the illumination is fully coherent, spatially and temporally, or any partial coherence of the illumination is removed in the reconstruction; 3) the beam-sample interaction fulfills the weak phase object approximation; and 4) the scanning error from the beam and sample drift is negligible with respect to the target resolution. However, in the real world, the detector cannot be infinite, the illumination is not fully coherent and there are always detection errors. Despite these practical limitation, many of these conditions can be partially ameliorated via suitable reconstruction algorithms or hardware improvements.

On the other hand, one of the largest benefits of conventional STEM is that it provides simultaneous access to a variety of imaging and analytical signals. For example, both structural and chemical information can be obtained by using annular shaped detectors to collect high-angle scattered electrons and simultaneously using an electron energy loss spectrometer to collect and analyze the small-angle scattering due to inelastic energy loss events.[18–21] However, in most current 4D-STEM setups, the detector used to collect the diffraction patterns is installed between the sample and the energy filter. While the detector collects nearly all of the scattered electrons, it blocks the electrons for electron energy loss spectroscopy (EELS) analysis, preventing simultaneous chemical analysis. Acquiring sequential images is certainly possible, but then drift, damage, or other factors that change over time may play a role. As a result, correlative structural imaging and chemical analysis become challenging.

Another advantage of ptychography, which has not yet been extensively explored, is that it does not need each of the diffraction patterns in the 4D dataset to be complete for the reconstruction.This allows for some measurements/pixels/units to be removed in the detector, providing opportunities to perform simultaneous 4D-STEM and EELS analysis. Studies in this direction, however, are rather limited. To our knowledge, only one paper has reported the ptychographic reconstruction of a data set of "hollow" diffraction patterns.[22] In that work, Song and colleagues used ptychography to reconstruct the phase of a monolayer sample and examine the effect of inner angle and probe-position error. This work was the first (our knowledge) journal publication that points out the potential for recovering both structural and chemical information using a hollow detector. Some investigation of a partial detector was also presented in the thesis of one of the present authors.[23] However, using a hollow detector for imaging bulk materials, that is, non-monolayer specimens, has not yet been explored. Although the associated hollow detectors are currently not available, we believe such a configuration represents a promising new direction for 4D-STEM and will provide further new opportunities for the analysis of materials, where a reliable correlation of local structure and chemical bonding is essential. In this work, we further demonstrate the feasibility of annular pixelated detector (APD) for simultaneous 4D-STEM and EELS by performing systematic analysis and comprehensive evidence using a bulk specimen. We also examine detectors with asymmetric geometries and find that atomic resolution ptychography is robust to detector defects or potential misalignment to the EEL spectrometer or the diffraction pattern. We demonstrate that general structural reconstruction is feasible even when a substantial fraction of the central disk is blocked, which means that simultaneous ptychographic structure imaging and EELS are possible.

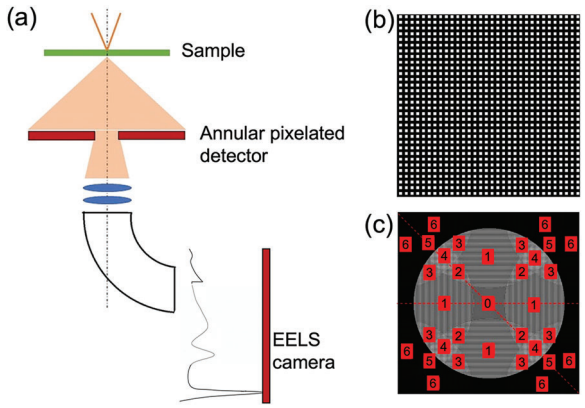

Figure 1. a) Schematic illustration of a simplified version of the combination of an annular pixelated detector and an EELS detector. b) The binary phase structure of the model, which simulates a single crystal sample; and c) one of the calculated diffraction patterns, (reproduced from Author's thesis[23]). Numbers in red boxes indicate the number of overlapping beams.

2. Results and Discussion

The design concept of integrating an annular pixelated direct electron counting camera in a STEM to enable both 4D STEM acquisition and EELS analysis is shown schematically in **Figure 1**a. The 4D detector is configured as a conventional direct electron detector with detection units in the central region removed to let part of the central beam pass through to the EELS detector. The ratio δ between the removed area r_{off} and the area of the whole central disc r can be controlled by the convergence angle or the camera length (the distance between the sample and the 4D detector). For example, a larger convergence angle gives a larger central disc, making δ smaller, as does increasing the optical distance between the sample and the 4D detector. Clearly both of these factors or other lens strengths can be varied to obtain the desired optical configuration.

$$\delta = r_{off}/r \tag{1}$$

This annular detector setup allows the acquisition of a set of 4D hollow diffraction patterns, while a fraction of the electrons in the central disc reach the entrance aperture for EELS analysis. Acquisition synchronization between the 4D detector and the EEL spectrometer thus allows simultaneous acquisition of hollow diffraction patterns and EELS as a function of probe position on the specimen. The 4D hollow diffraction patterns can be processed by ptychography to extract the complex transmission function (structure information) of the sample, while EELS analysis gives the chemical information.

Critical questions include: How many electrons does ptychography need for atomic scale reconstruction and how many

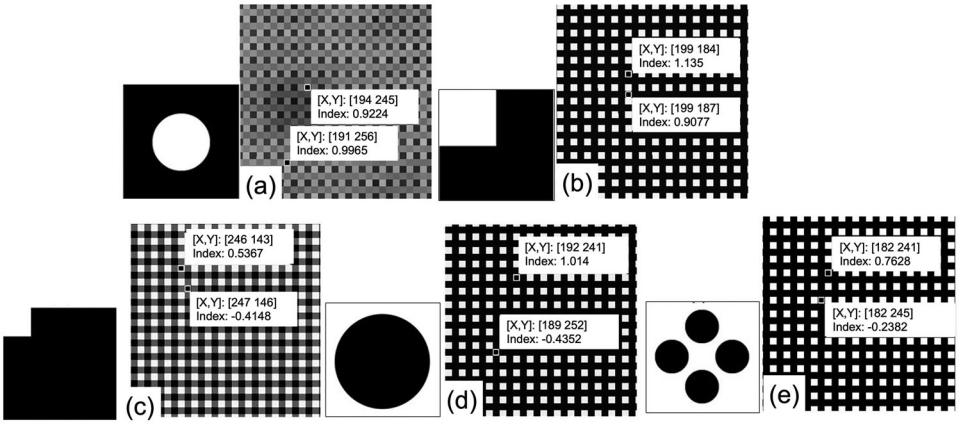

Figure 2. Different masks applied to the diffraction patterns to simulate a partial detector and their corresponding phase reconstructions. a) All electrons are blocked except half of the diameter region of the center disk; only b) the upper top quarter and c) 1/16 corner of the detector are used for the reconstruction; d) the entire center disk is blocked; and e) electrons in four small circles are blocked. Inset text boxes indicate the coordinates and relative intensities of selected pixels in the reconstruction.

electrons are enough for the EELS analysis? Do electrons at symmetric scattering angles have to be included to generate a sensible reconstruction? Are we still able to reconstruct the atomic structure of the specimen when some randomly positioned pixels on the detector are dead? To address some of these questions, we performed various simulations based on both simulated and experimental data. Results show that ptychography can reconstruct atomic structures for either monolayer or bulk specimens without losing critical information, until most of the central disc is blocked.

We first tested simulated diffraction patterns from a monolayer array structure in order to figure out the minimum pixels needed for ptychographic reconstruction and to evaluate if a symmetric shaped detector is required. The phase of the simulated crystal is shown in Figure 1b, and a representative diffraction pattern is shown in Figure 1c. Diffraction patterns were simulated by assuming the sample is placed at a defocused illumination plane. A hundred diffraction patterns from 10×10 grid scanning positions were generated in each dataset. In order to assess the impact of shapes of the hollow in the detector, binary (1/0) masks with different geometries were used to generate partial diffraction patterns and the corresponding phase reconstructions from these masks are shown in **Figure 2**a–e. The zeros in the masks represent the removed pixels on the detector. Figure 2a shows that when the collection angle is half the convergence angle and only electrons in the very middle of the central disk are used, the atomic structure of the specimen is not well reconstructed, illustrating the importance of the collection angle in defining ptychography reconstructions. For all the other masks considered here, regardless of their shapes and positions, the structure of the model specimen is reasonably well recovered.

This result indicates several beneficial aspects of ptychography for structural reconstruction. First, the general reconstruction is quite robust to a hollow geometry, even when a large portion of the central diffraction is blocked. Second, the method shows good tolerance to the presence of defects in the detector. Third, the reasonable reconstruction from the asymmetric masks indicates that an overall reconstruction is possible in a practical setting when the hollow detector is not well aligned with the diffraction pattern or with the entrance aperture of the EELS spectrometer. Fourth, as Figure 2d highlights even when the entire central diffraction is blocked, the general features of this extremely simple structure can still be resolved.

These results of ptychography based on simulated partial diffraction patterns encourage us to simulate an annular pixelated camera, which collects annular diffraction patterns and allows EELS analysis simultaneously. We used 4D Canvas, a PN detector equipped on a JEOL NeoARM to acquire experimental 4D-STEM datasets at 80 kV. Datasets with various experimental conditions were acquired and processed by an advanced version of an algorithm based on the ePIE reconstruction method.[24]

A bulk $SrTiO_3$ single crystal along the [100] zone axis was used as the model material. The dataset was collected by positioning the sample at the focused plane. A sequence of 128×128 diffraction patterns were collected with a convergence angle of 40 mrad. A HAADF image was simultanusly collected during the scan. The modal decomposition algorithm (mPIE), developed from Wolf's modes decomposition of spatially partially coherent source theory,[25] was used in the reconstruction of the complete dataset presented in this work. A representative diffraction pattern and a simultaneously acquired HAADF image are shown in **Figures 3**a and 3b, respectively. The phase and modulus of the ptychographic reconstruction from the dataset with mPIE[26] are shown in Figures 3c and 3d, respectively. The dark contrast in Figure 3c is due to the amplitude, that is, absorption contrast. The reconstruction accounts for partial spatial incoherence by decomposing the probe function into a set of mutually independent orthogonal modes[26] , shown in Figure 3e. The overall crystalline structure is resolved in both reconstructed images (Figures 3c and 3d), indicating that ptychographic imaging of the lattice structure is feasible in this specimen and the 4D STEM dataset can be used to test the feasibility of using hollow detectors for ptychography imaging. However, we want to point out that in this particular case, the oxygen columns are not resolved in the ptychographic reconstruction, likely due to the relatively large scanning step size (0.4 Å) used in this experiment and the possibility of deviations from the zone axis in the specimen.

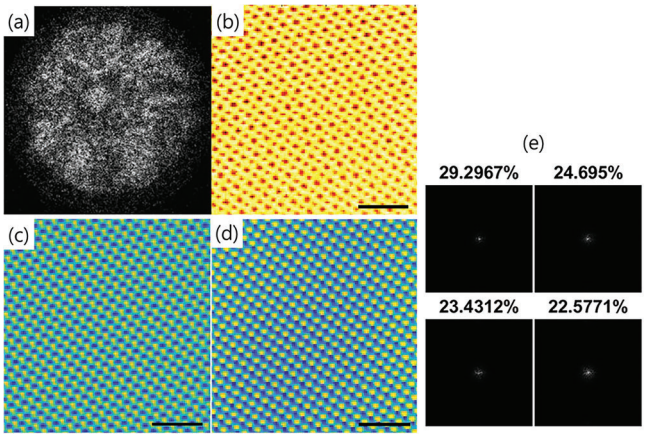

Figure 3. a) Representative diffraction pattern with a convergence angle of about 40mrad; the specimen is a single crystal STO along the [100] zone axis. b) The HAADF of the scanned area collected simultaneously with the 4D dataset. c,d) The modulus and phase of the ptychographic reconstruction from the complete dataset with the modal decomposition algorithm (mPIE), respectively. e) Four independent modes of the effective electron source, which arise from the reconstruction to account for the partial coherence. Scale bar is 1 nm.

Hollow diffraction patterns were generated by applying masks to each of the diffraction patterns. **Figure 4**a–e shows the masks and the corresponding diffraction patterns with a block angle of 1.8, 3.7, 18.5, 27.8, and 37 mrad, respectively. Figure 4f-k shows the phase reconstructions with a varying size ofthe hollow diffraction patterns. As visually apparent from this figure, even in the case of a large block angle, the reconstructed image is still qualitatively comparable to the simultaneously collected HAADF image. The reconstructed images are nearly identical for block angles between 1.8 and 27.8 mrad, corresponding to 75% of the convergence angle. This result indicates that blocking the majority of the central disk does not affect the ptychographic imaging of the atomic structure in this case. However, as the block angle approaches the convergence angle, especially in the 37 mrad case, the structure of the atomic columns starts to deteriorate. This suggests that ptychographic imaging becomes challenging only when most the central disk is blocked. These results also show that for bulk samples, ptychography has a considerable tolerance to missing pixels inside the central disc, which is due to the fact that most of the high-resolution structure information is encoded in the scattering at high angles.

To further validate hollow ptychography, we conducted simulations of both conventional STEM imaging and 4D-STEM datasets using Dr. Probe software.[27] We then compared the results of our simulations with our experimental findings to gain a better understanding of the technique's capabilities. The simulations utilize the same beam and specimen conditions as that of the experiments, that is, a convergence angle of 40 mrad, an acceleration voltage of 80 kV, a zone axis of [001] and a thickness of 5 nm of $SrTiO_3$, which was determined using position-averaged convergent beam electron diffraction (PACBED) simulations. In the ptychography scans, we used a step size of 0.335 Å with a total of 128 × 128 scanning positions, and padded each diffraction pattern with zeros to obtain a real-space pixel size of 0.25 Å. **Figure 5**a shows a representative PACBED of $SrTiO_3$ for the ptychography simulation using the ADF detector, a simulated HAADF image superimposed on an atomic model of $SrTiO_3$, and the ptychography reconstruction of the modulus and phase. The simulated results are consistent with our experimental results shown in Figure 3. We employed this atomic model into the ePIE algorithm with block angles of 3.7, 18.5, 27.8, and 37 mrad, as shown in Figure 5b–e, respectively.

To ensure a fair comparison between the reconstructed phase images, we displayed them using the phase range (Figure 6). Our analysis reveals that the reconstructed images are almost identical for block angles between 3.7 and 27.8 mrad, as shown in Figure 4. However, we observed that the atomic column intensity appears dimmer with increase of the block angle. Furthermore, the difference in the phase contrast between the Sr and Ti atoms becomes increasingly obscured as the block angle increases, as shown in Figure 5a,c. We also found that the weak phase contrast of O atoms deteriorates with the increase of the block angle. These results suggest that the size of the blocked angle affects the phase contrast and reflects the impact of the hollow detector on the phase. Despite these effects, our simulations show that the structural information can still be reconstructed accurately even when using block angles within a specific range. However, when the block angle approaches the convergence angle (≈40 mrad), the atomic columns appear erroneous and noisy. Overall, our simulation results are consistent with our experimental findings, further supporting the robustness of hollow ptychography for the structural analysis of thin samples. **6**.

To quantify the reconstruction, we used the Fourier ring correlation (FRC) to compare each of the hollow reconstructions with that reconstructed from the complete diffraction patterns (Figure 6. The FRC as a function of the radius (R) of the spatial frequency is defined as:

$$FRC\ (R) = \sum_{q=R} F_1(q)\, F_2^*(q) \Big/ \sqrt{\sum_{q=R} |F_1(q)|^2 \sum_{q=R} |F_2(q)|^2} \qquad (2)$$

where $F_1(q)$ and $F_2(q)$ are the Fourier transforms of two reconstructions.[28] The FRC measures the degree of correlation as a function of spatial frequency. The comparison of the FRC between the reconstructions of different block angles and that obtained from the complete diffraction patterns is shown in Figure 6a, , indicating that the reconstruction at each frequency degrades with the increase of the block angle. Figure 6b,c shows the Fourier transforms of the reconstructions for block angles of 1.8 and 37 mrad, respectively. Although the Bragg peaks from the block angle of 37 mrad are generally weaker, most of the Bragg peaks are visible in both cases. This result further confirms that the structural information is generally preserved even for large block angles,although the overall quality of the ptychographic reconstruction degrades, as shown in Figures 4k and 5e. Thus, a high block angle, such as 37 mrad, may be used to study structural symmetry but is not recommended for reconstructing atomic-scale amplitudes and phases.

The above results demonstrate that structural reconstruction by ptychography for 4D-STEM datasets acquired with a hollow or defective detector is feasible, even when a large portion of the central diffraction disk is used for the EELS analysis. This indicates the feasibility of simultaneous EELS analysis using the electrons in the central disk. However, it should be noted

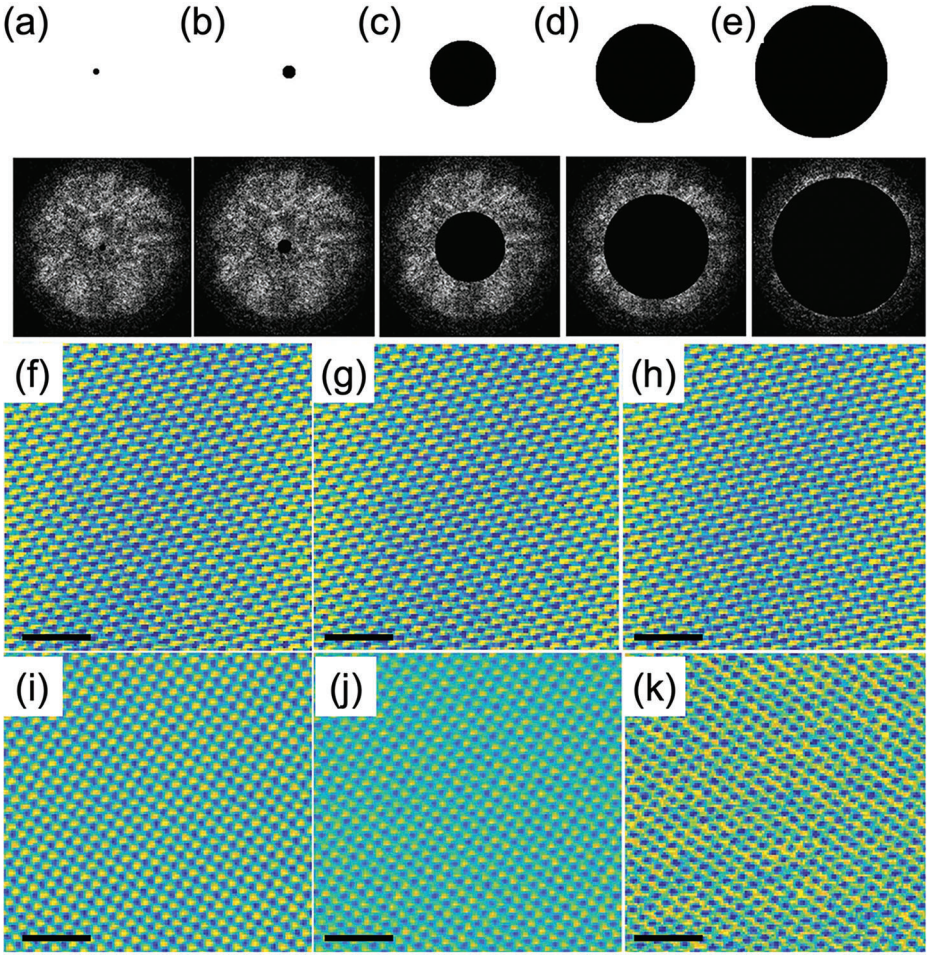

Figure 4. Detector masks and reconstructed images from a 4D-STEM dataset of $SrTiO_3$. a–e) Different sizes of masks with block angles of 1.8, 3.7, 18.5, 27.8, and 37 mrad applied to diffraction patterns. f–k) Phase reconstructions from f) complete diffraction patterns, and g–k) diffraction patterns with block angles corresponding to those in (a–e), respectively. Scale bar: 1 nm.

that such simultaneous 4D-STEM and EELS data acquisition does not work optimally in all scenarios. For example, for beam-sensitive materials, a reduced electron dose is often needed. Using an extremely fast scan or a defocused beam have been shown to reduce beam irradiation for organic materials without sacrificing spatial resolution or phase sensitivity,[29–31] but may not be ideal for EELS acquisition. The dose required for structural analysis via ptychography, especially for thin specimens, is usually lower than the dose required for atomic-resolution EELS. In the second scenario where a defocused electron probe is used, EELS analysis becomes challenging. Currently, no equivalent reconstruction algorithm is available for the EELS signal, so a broad beam would not allow for a pixel-by-pixel equivalent spectrum image to the high-spatial-resolution ptychography data. In these cases, separate acquisitions might still be needed in order to match the optimal experimental conditions for each technique. Future developments in hardware, theoretical simulations, and interpretations may help to overcome these challenges.

It should be also noted that the number of electrons needed for reconstructions varies significantly among specimens. Ptychography is a deconvolution method to solve the unknowns from the knowns, where the input data are the diffraction patterns which are given by the beam and specimen structure. Therefore, samples with different structure, thickness, elements, phase, require a different number of pixels for the reconstruction. Based on our results on a bulk $SrTiO_3$ specimen and previously reported MoS_2 monolayer,[22] it is reasonable to conclude that atomic structure reconstruction using ptychography is feasible when the majority of the central disk is blocked in both cases, while caution should be taken for phase reconstruction. Furthermore, while this work focuses on reconstruction using a single $SrTiO_3$ sample as a model system, the tolerance of ptychography for phase reconstruction using a hollow detector may vary for other samples and experimental conditions. Therefore, the selection of electrons to be collected by an annular 4D STEM detector may have to be chosen based on the specimen chemistry and thickness, and the specific information that one wants to obtain.

3. Conclusion

We have performed an evaluation of electron ptychography for atomic structure reconstruction using only a fraction of the scat-

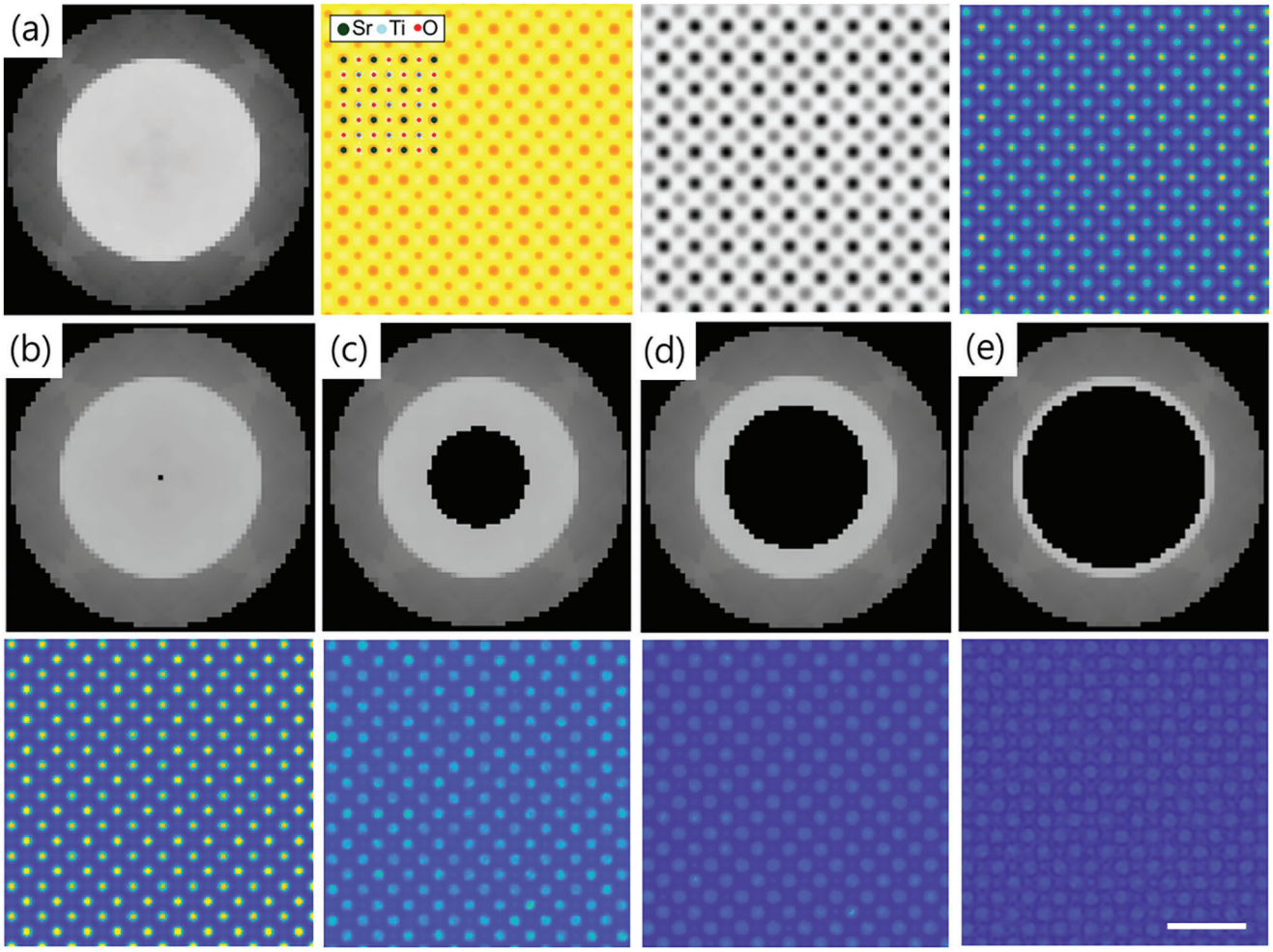

Figure 5. STEM images and ptychography simulation data set of $SrTiO_3$ by varying the size of the block mask on the diffraction patterns. a) Representative position averaged convergent beam electron diffraction (PACBED), a simulated HAADF image superimposed an atomic model of $SrTiO_3$, and the reconstructed modulus and phase from complete diffraction patterns. b–e) The ptychographic phase reconstruction from diffraction patterns with block angles of 3.7, 18.5, 27.8, and 37 mrad, respectively. Scale bar is 1 nm.

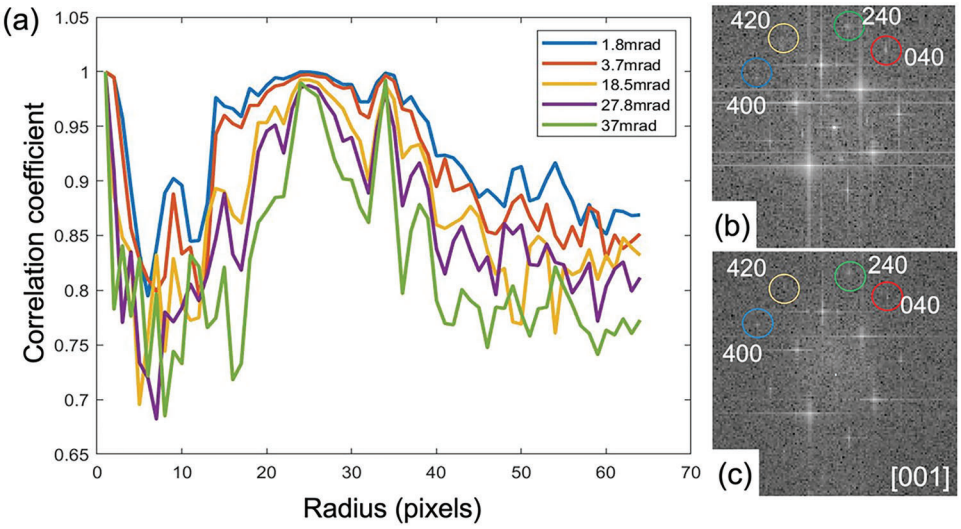

Figure 6. a) Fourier ring correlation comparison between the reconstructions of block angles of 1.8, 3.7, 18.5, 27.8, and 37 mrad and that obtained from the complete diffraction patterns. b,c) The Fourier transform of the reconstruction with block angles of b) 1.8 mrad and c) 37 mrad, with same Bragg peaks circled.

tered electrons. We found that electron ptychography is overall robust to the amount of scattered electrons used. The atomic structure information of specimens can be reconstructed even when a hollow detector, a detector with an asymmetric shape, or a detector with defective regions is used. It is also worth pointing out that the collection angle used in very high-energy resolution monochromated EELS is often only around 50% of the convergence angle[32] so that high-order aberrations do not degrade the energy resolution. Our results show that complete structural information of specimens can be extracted from incomplete diffraction patterns in 4D datasets, even when the majority of the central disk is blocked, demonstrating the feasibility of simultaneous EELS and electron ptychography. Phase reconstruction, however, is more sensitive to detector and specimen geometry, and experimental parameters should be carefully selected when using a hollow detector for phase reconstruction. We believe that an annular pixelated detector represents a promising future direction for STEM imaging hardware, allowing the acquisition of HAADF images, ptychographic reconstructions, and EELS datasets simultaneously.

Acknowledgements

This work was supported by the U.S. Department of Energy (DOE), Office of Basic Energy Sciences (BES), Division of Materials Sciences and Engineering and by the Center for Nanophase Materials Sciences, a U.S. DOE Office of Science User Facility at Oak Ridge National Laboratory. Some of the technique development was supported by a DOE-BES Early Career Award. Microscopy was conducted at the CNMS. NYK and SC contributed equally to this work.

Conflict of Interest

The authors declare no conflict of interest.

Data Availability Statement

The data that support the findings of this study are available from the corresponding author upon reasonable request.

Keywords

4D-scanning transmitting electron microscopy (STEM), electron energy loss spectroscopy (EELS), electron microscopy, electron ptychography, pixelated detectors

Received: December 26, 2022
Revised: April 13, 2023
Published online:

[1] C. Ophus, *Microsc. Microanal.* **2019**, *25*, 563.
[2] D. Muller, Z. Chen, Y. Jiang, M. Odstrcil, *Microsc. Microanal.* **2020**, *26*, 624.
[3] M. Krajnak, D. Mcgrouther, D. Maneuski, V. O' Shea, S. Mcvitie, *Ultramicroscopy* **2016**, *165*, 42.
[4] K. Müller-Caspary, M. Duchamp, M. Rösner, V. Migunov, F. Winkler, H. Yang, M. Huth, R. Ritz, M. Simson, S. Ihle, H. Soltau, T. Wehling, R. E. Dunin-Borkowski, S. Van Aert, A. Rosenauer, *Phys. Rev. B* **2018**, *98*, 121408.
[5] J. A. Hachtel, J. C. Idrobo, M. Chi, *Adv. Struct. Chem. Imaging* **2018**, *4*, 10.
[6] V. Boureau, M. Staňo, J. L. Rouviere, J. C. Toussaint, O. Fruchart, D. Cooper, *J. Phys. D Appl. Phys.* **2021**, *54*, 085001.
[7] Q. Zheng, T. Feng, J. A. Hachtel, R. Ishikawa, Y. Cheng, L. Daemen, J. Xing, J. C. Idrobo, J. Yan, N. Shibata, Y. Ikuhara, B. C. Sales, S. T. Pantelides, M. Chi, *Sci. Adv.* **2021**, *7*, eabe6819.
[8] H. Yang, T. J. Pennycook, P. D. Nellist, *Ultramicroscopy* **2015**, *151*, 232.
[9] M. J. Zachman, Z. Yang, Y. Du, M. Chi, *ACS Nano* **2022**, *16*, 1358.
[10] M. J. Zachman, J. Madsen, X. Zhang, P. M. Ajayan, T. Susi, M. Chi, *Small* **2021**, *17*, 2170142.
[11] H. Yang, R. N. Rutte, L. Jones, M. Simson, R. Sagawa, H. Ryll, M. Huth, T. J. Pennycook, M. L. H. Green, H. Soltau, Y. Kondo, B. G. Davis, P. D. Nellist, *Nat. Commun.* **2016**, *7*, 12532
[12] L. Zhou, J. Song, J. S. Kim, X. Pei, C. Huang, M. Boyce, L. Mendonça, D. Clare, A. Siebert, C. S. Allen, E. Liberti, D. Stuart, X. Pan, P. D. Nellist, P. Zhang, A. I. Kirkland, P. Wang, *Nat. Commun.* **2020**, *11*, 2773.
[13] Y. Jiang, Z. Chen, Y. Han, P. Deb, H. Gao, S. Xie, P. Purohit, M. W. Tate, J. Park, S. M. Gruner, V. Elser, D. A. Muller, *Nature* **2018**, *559*, 343.
[14] A. R. Lupini, M. Chi, S. Jesse, J. Microsc, *J. Microsc.* **2016**, *263*, 43.
[15] J. Rodenburg, *Nature* **2018**, *559*, 334.
[16] M. J. Humphry, B. Kraus, A. C. Hurst, A. M. Maiden, J. M. Rodenburg, *Nat. Commun.* **2012**, *3*, 730.
[17] J. Miao, T. Ishikawa, I. K. Robinson, M. M. Murnane, *Science* **2015**, *348*, 530.
[18] C. Ma, Y. Cheng, K. Yin, J. Luo, A. Sharafi, J. Sakamoto, J. Li, K. L. More, N. J. Dudney, M. Chi, *Nano Lett.* **2016**, *16*, 7030.
[19] M. J. Zachman, J. A. Hachtel, J. C. Idrobo, M. Chi, *Angew. Chem.* **2020**, *132*, 1400.
[20] S. J. Pennycook, P. D. Nellist, **,** https://doi.org/10.1007/978-1-4419-7200-2.
[21] X. Liu, R. Garcia-Mendez, A. R. Lupini, Y. Cheng, Z. D. Hood, F. Han, A. Sharafi, J. C. Idrobo, N. J. Dudney, C. Wang, C. Ma, J. Sakamoto, M. Chi, *Nat. Mater.* **2021**, *20*, 1485.
[22] B. Song, Z. Ding, C. S. Allen, H. Sawada, F. Zhang, X. Pan, J. Warner, A. I. Kirkland, P. Wang, *Phys. Rev. Lett.* **2018**, *121*, 146101.
[23] S. Cao, Ph.D. Thesis, University of Sheffield **2017**.
[24] D. Johnson, P. Li, A. Maiden, *Optica* **2017**, *4*, 736.
[25] E. Wolf, *Opt. Commun.* **1981**, *38*, 3.
[26] S. Cao, P. Kok, P. Li, A. M. Maiden, J. M. Rodenburg, *Phys. Rev. A* **2016**, *94*, 063621.
[27] J. Barthel, *Ultramicroscopy* **2018**, *193*, 1.
[28] M. van Heel, *Ultramicroscopy* **1987**, *21*, 95.
[29] J. G. Lozano, G. T. Martinez, L. Jin, P. D. Nellist, P. G. Bruce, *Nano Lett.* **2018**, *18*, 6850.
[30] G. Li, H. Zhang, Y. Han, *ACS Cent. Sci.* **2022**, *8*, 1579.
[31] Z. Chen, M. Odstrcil, Y. Jiang, Y. Han, M. H. Chiu, L. J. Li, D. A. Muller, *Nat. Commun.* **2020**, *11*, 2994.
[32] J. A. Hachtel, A. R. Lupini, J. C. Idrobo, *Sci. Rep.* **2018**, *8*, 5637.

